RESEARCH ARTICLE SUMMARY

STRUCTURAL BIOLOGY

Structural basis of Nav1.7 inhibition by an isoform-selective small-molecule antagonist

Shivani Ahuja, Susmith Mukund, Lunbin Deng, Kuldip Khakh, Elaine Chang, Hoangdung Ho, Stephanie Shriver, Clint Young, Sophia Lin, J. P. Johnson Jr., Ping Wu, Jun Li, Mary Coons, Christine Tam, Bobby Brillantes, Honorio Sampang, Kyle Mortara, Krista K. Bowman, Kevin R. Clark, Alberto Estevez, Zhiwei Xie, Henry Verschoof, Michael Grimwood, Christoph Dehnhardt, Jean-Christophe Andrez, Thilo Focken, Daniel P. Sutherlin, Brian S. Safina, Melissa A. Starovasnik, Daniel F. Ortwine, Yvonne Franke, Charles J. Cohen, David H. Hackos,* Christopher M. Koth,* Jian Payandeh*

INTRODUCTION: Voltage-gated sodium (Nav) channels open and close ion-selective pores in response to changes in membrane potential, and this gating underlies the generation of action potentials. Nav channels are large membrane proteins that contain four peripheral voltage-sensor domains (VSD1–4) that influence the functional state of the central ion-conducting pore. Mutations within the nine human Nav channel isoforms are associated with migraine (Nav1.1), epilepsy (Nav1.1–1.3, Nav1.6), pain (Nav1.7–1.9), cardiac (Nav1.5), and muscle paralysis (Nav1.4) syndromes. Accordingly, Nav channel blockers are used for the treatment of many neurological and cardiovascular disorders. These drugs bind within the central pore domain and generally lack isoform selectivity owing to the high sequence conservation found among Nav channels, limiting their therapeutic utility. In this study, we focused on a recently identified class of isoform-selective small-molecule antagonists that target a unique binding site on the fourth voltage-sensor domain, VSD4. Here we report the structural determination of such small-molecule aryl sulfonamide antagonists in complex with human Nav1.7 VSD4. Our studies demonstrate how this important new class of gating modifier engages VSD4 to inhibit Nav channel activity through a "voltage-sensor trapping" mechanism.

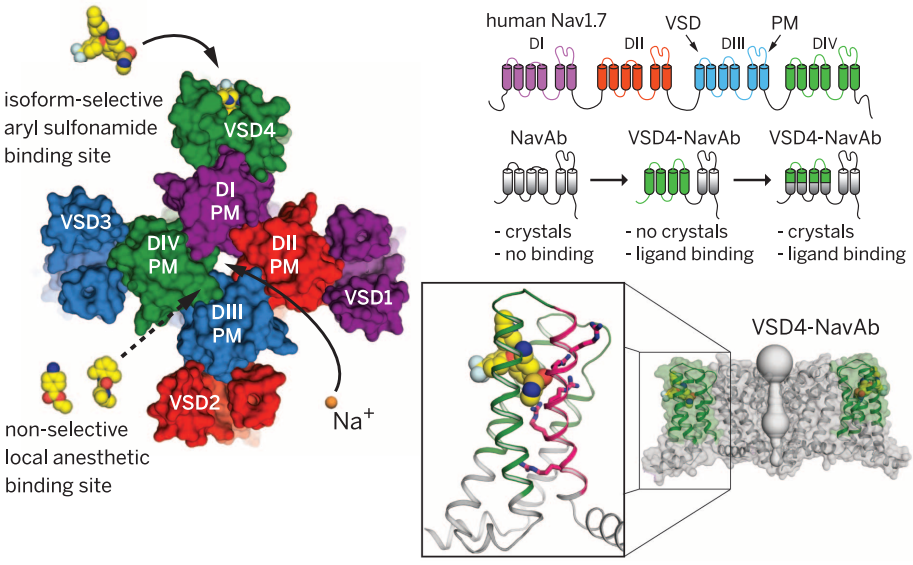

Drug binding sites in sodium channels. (**Left**) Top-view model of human Nav1.7. When open, sodium passes through the channel. Blocking drugs lacking isoform selectivity bind to a conserved site within the central pore. Isoform-selective inhibitors bind to a distinct site on VSD4. (**Right**) Strategy for Nav1.7 crystallography. Portions of Nav1.7 VSD4 were grafted onto a tetrameric channel (NavAb) and crystallized. (**Inset**) Side view of aryl sulfonamide binding site with the S4 helix and arginine gating charges highlighted pink.

RATIONALE: For structural studies, we devised a novel protein-engineering strategy that overcomes the technical complexities of producing full-length human Nav channels. Exploiting the evolutionary relationship between human and bacterial Nav channels, we fused portions of Nav1.7 VSD4 onto the bacterial channel NavAb. Using ligand-binding assays and alanine-scanning mutagenesis, we demonstrated that the antagonist binding site present in the human Nav1.7 channel is preserved within this human VSD4-NavAb chimeric channel. This chimeric construct allowed purification, crystallization, and structure determination of potent aryl sulfonamide antagonists in complex with the human Nav1.7 VSD4 binding site.

RESULTS: Functional studies using patch-clamp electrophysiology revealed that aryl sulfonamide inhibitors bind with high affinity to an isoform-selective and extracellularly accessible site on VSD4. These inhibitors show a high level of state dependence, potently blocking human Nav1.7 only when VSD4 is in its activated conformation. Our crystallographic studies revealed that the anionic warhead from the aryl sulfonamide inhibitors directly engages the fourth gating charge residue (R4) on the voltage-sensing S4 helix, effectively trapping VSD4 in its activated state. Isoform selectivity is achieved by inhibitor interactions with nonconserved residues found on the S2 and S3 transmembrane helices. The drug receptor site is partially submerged within the membrane bilayer, and a peripherally bound phospholipid was observed to form a tripartite complex with the antagonist and channel.

ON OUR WEB SITE

Read the full article at http://dx.doi.org/10.1126/science.aac5464

CONCLUSION: A new crystallization strategy has enabled the structural determination of VSD4 from human Nav1.7 in complex with potent, state-dependent, isoform-selective small-molecule antagonists. Mechanistically, inhibitor binding traps VSD4 in an activated conformation, which stabilizes a nonconductive state of the channel, and likely prevents recovery from inactivation. Unique phospholipid interactions and an exposed inhibitor binding site expand the importance of the membrane bilayer in ion channel biology. We anticipate that these structures will enable drug design efforts aimed at other voltage-gated ion channels and may accelerate the development of new treatments for pain that selectively target Nav1.7. ■

The list of author affiliations is available in the full article online.
*Corresponding author. E-mail: hackos.david@gene.com (D.H.H.); koth.christopher@gene.com (C.M.K.); payandeh.jian@gene.com (J.P.)
Cite this article as S. Ahuja *et al.*, *Science* **350**, aac5464 (2015). DOI: 10.1126/science.aac5464

Downloaded from http://science.sciencemag.org/ on February 26, 2020

RESEARCH ARTICLE

STRUCTURAL BIOLOGY

Structural basis of Nav1.7 inhibition by an isoform-selective small-molecule antagonist

Shivani Ahuja,[1]*† Susmith Mukund,[1]* Lunbin Deng,[2]‡ Kuldip Khakh,[3]‡ Elaine Chang,[3]‡ Hoangdung Ho,[1] Stephanie Shriver,[1] Clint Young,[3] Sophia Lin,[3] J. P. Johnson Jr.,[3] Ping Wu,[1] Jun Li,[4] Mary Coons,[1]§ Christine Tam,[1] Bobby Brillantes,[1] Honorio Sampang,[1] Kyle Mortara,[1] Krista K. Bowman,[1] Kevin R. Clark,[5] Alberto Estevez,[1] Zhiwei Xie,[3] Henry Verschoof,[3] Michael Grimwood,[6] Christoph Dehnhardt,[6] Jean-Christophe Andrez,[6] Thilo Focken,[6] Daniel P. Sutherlin,[4] Brian S. Safina,[4] Melissa A. Starovasnik,[1] Daniel F. Ortwine,[4] Yvonne Franke,[1] Charles J. Cohen,[3] David H. Hackos,[2]‖ Christopher M. Koth,[1]‖ Jian Payandeh[1]‖

Voltage-gated sodium (Nav) channels propagate action potentials in excitable cells. Accordingly, Nav channels are therapeutic targets for many cardiovascular and neurological disorders. Selective inhibitors have been challenging to design because the nine mammalian Nav channel isoforms share high sequence identity and remain recalcitrant to high-resolution structural studies. Targeting the human Nav1.7 channel involved in pain perception, we present a protein-engineering strategy that has allowed us to determine crystal structures of a novel receptor site in complex with isoform-selective antagonists. GX-936 and related inhibitors bind to the activated state of voltage-sensor domain IV (VSD4), where their anionic aryl sulfonamide warhead engages the fourth arginine gating charge on the S4 helix. By opposing VSD4 deactivation, these compounds inhibit Nav1.7 through a voltage-sensor trapping mechanism, likely by stabilizing inactivated states of the channel. Residues from the S2 and S3 helices are key determinants of isoform selectivity, and bound phospholipids implicate the membrane as a modulator of channel function and pharmacology. Our results help to elucidate the molecular basis of voltage sensing and establish structural blueprints to design selective Nav channel antagonists.

Voltage-gated sodium (Nav) channels conduct ionic currents that initiate action potentials in neurons and muscle cells. Consequently, Nav channels are the molecular targets of neurotoxins, clinically relevant drugs, and disease-causing mutations (*1*, *2*). Nav and voltage-gated calcium (Cav) and potassium (Kv) channels share a conserved architecture with a central ion-conducting pore module surrounded by four voltage-sensing domains (VSDs) (*2*, *3*). These remarkable proteins open and close ion-selective pores in response to small changes in membrane voltage, and their orchestrated gating underlies the generation of action potentials. In accordance with their specialized role in electrical signaling, Nav channels display rapid activation and fast inactivation properties (*1*, *2*). However, fundamental questions about their structure, pharmacological modulation, and functional relationship with the membrane bilayer persist.

Humans express nine closely related Nav channel isoforms (Nav1.1–1.9) that are differentiated by unique functional characteristics and tissue distribution patterns (*4*). The Nav1.7 channel is found almost exclusively in the peripheral nervous system, where it is highly expressed in olfactory epithelium, sympathetic ganglion, and dorsal root ganglion sensory neurons (*5*). Gain-of-function mutations in Nav1.7 are associated with extreme pain disorders (*6*, *7*), whereas loss-of-function mutations cause congenital insensitivity to pain in individuals who are otherwise free of motor or cognitive impairment (*8*, *9*). These contrasting phenotypes identify Nav1.7 as a key target in the pain perception pathway and have motivated intense efforts to develop selective inhibitors that are expected to overcome the liabilities of current analgesics.

The inherent complexity of mammalian Nav channels limits our ability to pursue crystallographic studies because these proteins contain a large pore-forming α subunit (~2000 residues) that undergoes extensive post-translational modification and associates with auxiliary subunits (*2*–*4*). By contrast, high-resolution structures of the biochemically more tractable homotetrameric Kv and bacterial Nav channels have been determined (*10*–*14*). Compared to Kv1.2 (*11*), the NavAb channel from *Arcobacter butzleri* has revealed distinct structural characteristics suggested to be shared with its human counterparts (*12*, *13*). However, experimental structures of mammalian Nav channels will be essential to understanding their distinctive functions, complex pharmacology, and precise relationship to bacterial Nav channels (*3*).

Architecturally, the α subunit of a mammalian Nav channel contains 24-transmembrane (TM) segments linked in four homologous domains (DI–DIV), where each domain contains six TM segments (S1–S6) (*2*, *4*). The S1–S4 segments form the four peripheral voltage-sensing domains (VSDs), which are distinct in primary sequence (VSD1–4). Each VSD is capable of sensing changes in the membrane voltage by virtue of positively charged arginine residues conserved along the S4 helix, and it is believed that the S4 helix translates within the VSD during voltage sensing (*15*, *16*). The S5 and S6 segments associate to form the ion-conducting pore module (PM) that scaffolds the selectivity filter and holds two pharmacologically important vestibules. The outer vestibule contains the binding sites for pore-blocking neurotoxins like tetrodotoxin (*17*), whereas the inner vestibule houses the therapeutically relevant local anesthetic receptor site (*18*).

All Nav channel inhibitors currently used in the clinic bind within the inner vestibule to prevent sodium conductance (*19*, *20*). Although block is state-dependent and generally thought to stabilize inactivated states of the channel (*21*–*23*), these inhibitors lack molecular selectivity among the Nav1.1–1.9 isoforms owing to the high sequence conservation found within the PM (*3*, *4*). Isoform-selective peptide toxins that target the outer vestibule are known (*24*, *25*), but these inhibitors lack state dependence and are unsuitable for oral dosing. To date, efforts to identify drugs with higher therapeutic index that target a receptor site offering improved isoform selectivity have failed (*26*, *27*). In this respect, peptide toxins that target the VSDs of Nav channels have generated considerable interest because these so-called gating modifiers profoundly affect the activation or inactivation properties of the channel (*28*, *29*), and isoform-selective toxins have been identified (*30*). Unfortunately, gating modifier toxins typically display poor drug-like properties, and clinical efficacy with these VSD-targeting molecules has yet to be demonstrated in humans.

A recent breakthrough study reported an aryl sulfonamide antagonist (PF-04856264) that binds to VSD4 and demonstrates molecular selectivity for human Nav1.7 over a subset of other Nav channel isoforms (*31*). Here, we describe the structural basis of Nav1.7 inhibition by this class of small-molecule antagonist using x-ray crystallography, and thus present important experimental structures of a small-molecule gating modifier in complex with a voltage-gated ion channel. Our study reveals the details of how an isoform-selective

[1]Department of Structural Biology, Genentech Inc., South San Francisco, CA 94080, USA. [2]Department of Neuroscience, Genentech Inc., South San Francisco, CA 94080, USA. [3]Department of Biology, Xenon Pharmaceuticals Inc., Burnaby, British Columbia, V5G 4W8, Canada. [4]Department of Discovery Chemistry, Genentech Inc., South San Francisco, CA 94080, USA. [5]Department of Biochemical and Cellular Pharmacology, Genentech Inc., South San Francisco, CA 94080, USA. [6]Department of Chemistry, Xenon Pharmaceuticals Inc., Burnaby, British Columbia, V5G 4W8, Canada.
*These authors contributed equally to this work. †Present address: Vollum Institute, Portland, OR 97239, USA. ‡These authors contributed equally to this work. §Present address: Caribou Biosciences, Berkeley, CA 94710, USA. ‖Corresponding author. E-mail: hackos.david@gene.com (D.H.H.); koth.christopher@gene.com (C.M.K.); payandeh.jian@gene.com (J.P.)

Downloaded from http://science.sciencemag.org/ on February 26, 2020

antagonist binds to VSD4 in a membrane environment to inhibit Nav1.7 (movie 1), and therefore highlights VSDs as untapped potential therapeutic targets (*32*–*34*). To enable these unique mammalian Nav channel crystal structures, we exploited the established portability of VSDs (*11*, *35*–*37*) and the presumed structural relatedness between human and bacterial Nav channels (*3*) to develop a robust protein production and crystallization strategy.

Characterization of small-molecule Nav1.7-selective gating modifiers

To investigate the nature of Nav1.7 inhibition by the aryl sulfonamide class of antagonists like PF-04856264, GX-674, and GX-395 (Fig. 1A) (*31*, *38*), we performed patch-clamp analysis of human Nav channels expressed in human embryonic kidney 293 (HEK293) cells. Using a representative compound of this class, GX-674, and a voltage protocol that allows Nav1.7 current measurements at both hyperpolarizing and depolarizing holding

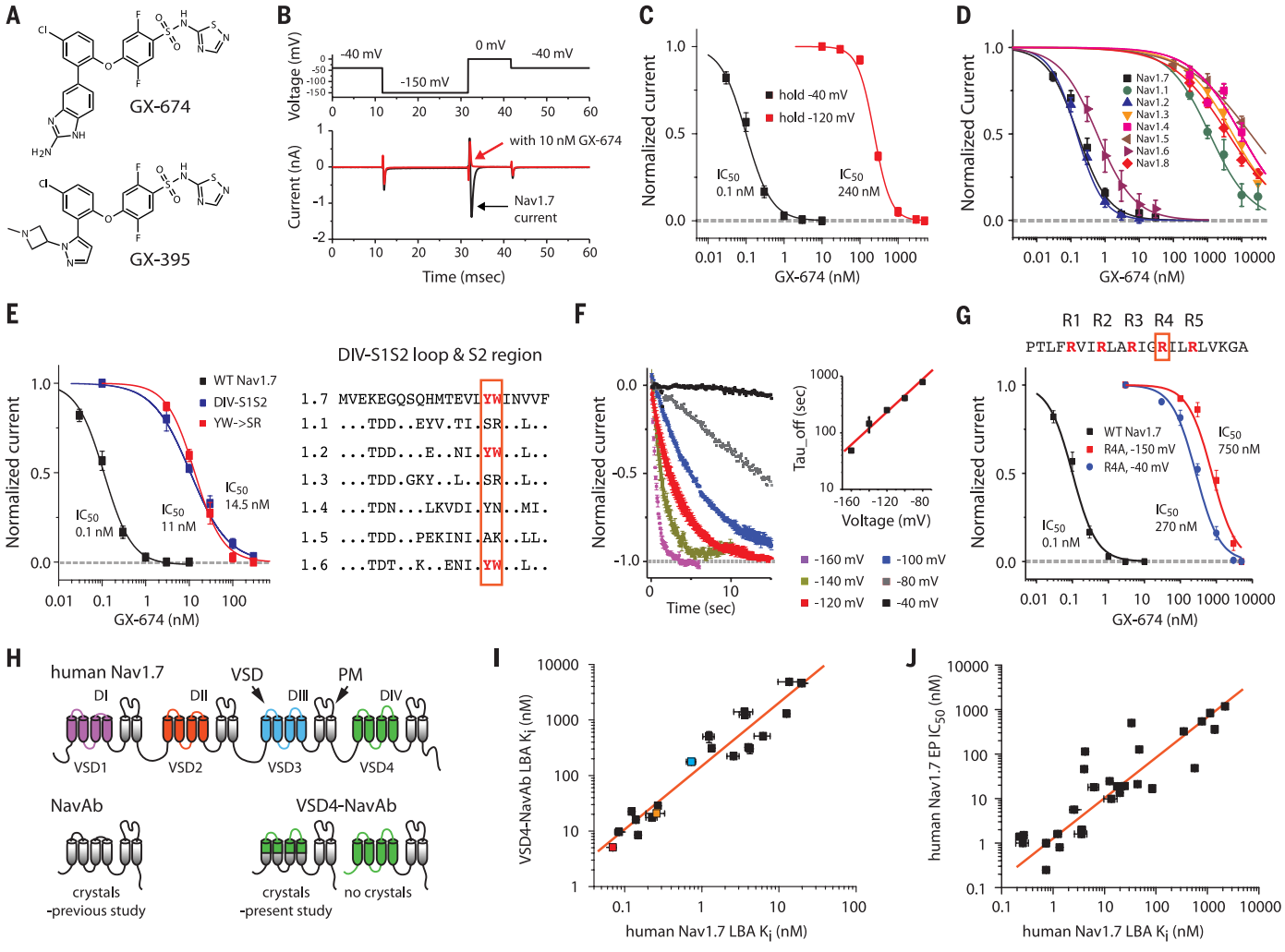

Fig. 1. Aryl sulfonamides inhibit native Nav1.7 and bind to chimeric VSD4-NavAb channels with high affinity. (**A**) Chemical structures of GX-674 and GX-395. GX-674 was found to have favorable properties for easier use in electrophysiological experiments. (**B**) Standard voltage protocol used for IC_{50} studies of human Nav1.7 (see Methods for further details). To enable current measurements at both hyperpolarizing and depolarizing holding voltages, a short 20-ms pulse to –150 mV was used to recover channels from inactivation, followed by a 10-ms pulse to 0 mV to open unblocked channels, which we repeated at 1-Hz frequency. Current traces using this voltage protocol are shown both in the absence (black) and presence (red) of 10 nM GX-674. (**C**) Dose-response curves of GX-674 on human Nav1.7 at holding potentials of –40 and –120 mV. For all electrophysiology data: $n \geq 3$, error bars indicate SEM, and IC_{50}'s are calculated with the Hill function. (**D**) Potency of GX-674 inhibition on a panel of human Nav channels (see Methods for further details). (**E**) A DIV-S1S2-Nav1.1 chimera and Y1537S/W1538R mutants in Nav1.7 VSD4 reduce GX-674 potency compared to wild-type Nav1.7 channels [see (B), holding voltage of –40 mV for each channel]. A sequence alignment between human Nav isoforms shows the S1-S2 loop and extracellular S2 region within VSD4. (**F**) Measurement of the off-rate following complete block with 10 nM GX-674 demonstrates a high degree of voltage dependence. Peak Nav current was measured over time with our standard voltage protocol (B), but at a frequency of 0.2 Hz and with more hyperpolarizing holding voltages as indicated. Time constants are shown in the inset. (**G**) The R1608A (R4A) mutation reduces the potency and state-dependence of block [see (B)]. The amino acid sequence of VSD4 S4 is shown for reference. (**H**) Domain architecture of the human Nav1.7 pore-forming α subunit and the simplier homotetrameric NavAb bacterial channel are illustrated. A schematic of the VSD4-NavAb chimeric channels used in the present study is also shown (sequence details found in fig. S3 and Methods). (**I**) A panel of 20 diverse aryl sulfonamide compounds were studied by radioligand-binding assays using [^{3}H]GX-545 on the native human Nav1.7 channel and the crystallization construct VSD4-NavAb (see fig. S3C and Methods for construct details). Select compounds used throughout this study are highlighted: [^{3}H]GX-545 (red), GX-674 (blue), and GX-936 (orange). The solid line indicates a linear regression to the observed data with a correlation coefficient of 0.956. (**J**) A panel of 28 diverse aryl sulfonamides were studied on the full-length human Nav1.7 channel using either radioligand binding with [^{3}H]GX-545 and automated patch-clamp electrophysiology. The solid line indicates a linear regression to the observed data with a correlation coefficient of 0.868. The full list of compounds used to generate the data presented in (I) and (J) are shown in tables S1 and S2.

Downloaded from http://science.sciencemag.org/ on February 26, 2020

voltages (Fig. 1B and fig. S1, A to C), we observed potent inhibition when GX-674 binding was equilibrated at −40 mV [half-maximal inhibitory concentration (IC_{50}) = 0.1 nM; Fig. 1C], a membrane voltage that promotes steady-state inactivation of Nav1.7. By contrast, GX-674 inhibition was weaker by a factor of 2400 at −120 mV (Fig. 1C), a voltage that promotes a resting closed state of the channel. A similar state dependence of block has been observed by local anesthetics that bind within the conserved inner vestibule of Nav channels (*19*), but unlike local anesthetics, GX-674 shows substantial Nav subtype selectivity, inhibiting Nav1.7 with much higher potency than most other Nav isoforms: Nav1.7 ~ Nav1.2 > Nav1.6 >> Nav1.1 > Nav1.8 > Nav1.3 > Nav1.4 ~ Nav1.5 (Fig. 1D). Notably, the potency of GX-674 for Nav1.7 is 100,000 times greater than that of the cardiac isoform Nav1.5 (*4*), which is a desirable property for cardiac safety and a level of selectivity unseen among local anesthetics.

Previous studies have shown that PF-04856264 and related aryl sulfonamides interact with the extracellular surface of VSD4 (*31*). To evaluate this conclusion, we first studied GX-395 (Fig. 1A) and its membrane-impermeant quaternary amine derivative GX-626, and observed that both compounds had similar potency and kinetics of Nav1.7 inhibition when applied extracellularly (fig. S2, A to C). In contrast to the membrane-impermeant local anesthetic QX-314 (*18*), GX-626 failed to inhibit Nav1.7 upon intracellular application (fig. S2D), pointing to an extracellular interaction site on the channel. To further validate the binding site of GX-674, we generated a Nav1.7 chimera in which the extracellular S1-S2 loop region of VSD4 was replaced with Nav1.1 sequence, which resulted in a factor of 100 decrease in potency (Fig. 1E). Indeed, modifying only two residues on the predicted extracellular side of the S2 helix to Nav1.1 or Nav1.3 equivalents (Y1537S/W1538R; Fig. 1E) resulted in a reduction in GX-674 potency by more than a factor of 100, pinpointing important determinants of isoform-selectivity on the extracellular face of VSD4 (fig. S3A). We also found that complete inhibition of Nav1.7 by GX-674 at −40 mV could be subsequently relieved by applying strong hyperpolarizing voltages (Fig. 1F and fig. S1D), suggesting a voltage-dependent deformation of the small-molecule receptor site. Because cysteine accessibility studies have demonstrated that gating charges can translocate from the intracellular side to the extracellular side of VSD4 during activation (*39*), we considered that Nav1.7 inhibition might involve an interaction between the negatively charged aryl sulfonamide warhead (Fig. 1A) and a positively charged S4 arginine side chain (Fig. 1G). Mutagenesis revealed that the R1608A (R4A) substitution decreased GX-674 potency by a factor of 3000 (Fig. 1G), indicating that R4 may translocate into the extracellular cleft of VSD4 during channel activation and make direct contact with GX-674. Consistent with this hypothesis, R4 is necessary for the state dependence of GX-674 inhibition, because this characteristic is almost completely eliminated in the R4A mutant channel (Fig. 1G).

Our data collectively indicate that GX-674 binds to a high-affinity, isoform-selective, and extracellularly accessible site on VSD4. Because GX-674 potently inhibits Nav1.7 only when VSD4 is in an activated conformation (Fig. 1C) and strong hyperpolarizations disrupt the receptor site (Fig. 1F and fig. S1D), we propose that binding of GX-674 opposes VSD4 deactivation. Since VSD4 activation is necessary and sufficient to produce fast inactivation (*16*, *40*), GX-674 binding may promote or stabilize an inactivated state of Nav1.7 through a VSD4-based voltage-sensor trapping mechanism. This mechanism is distinct from the α-scorpion and sea anemone gating modifier toxins that also bind to the surface of VSD4, because these toxins stabilize a deactivated conformation of VSD4 and slow the rate of fast inactivation (*28*, *41*). Moreover, and in contrast to canonical peptide gating modifiers like Protoxin-II that inhibit Nav channels but still allow some level of channel activation (*42*), GX-674 effectively abolishes channel activation between −80 mV and +60 mV when bound to Nav1.7 (fig. S4, A to D).

Protein engineering enables crystallization of Nav1.7 VSD4

To further understand the mechanism by which aryl sulfonamides antagonize Nav channels, we sought to determine crystal structures of human Nav1.7 VSD4 in complex with representative inhibitors. Because VSDs are modular protein domains that can be transferred en masse or in part onto distantly related channels while retaining their functional, pharmacological, and structural properties (*11*, *35*–*37*, *43*), we reasoned that the bacterial NavAb channel might facilitate the expression, purification, and crystallization of VSD4 and overcome the formidable challenges of producing full-length Nav1.7 for crystallization studies. The extracellular VSD loops in existing NavAb structures lack direct crystal contacts (*12*, *13*), suggesting that large sequence changes might be readily tolerated (fig. S5, A and B). The NavAb PM also forms a dominant crystal contact that we hoped would nucleate crystal growth (fig. S5C).

We began by replacing the NavAb VSD with each of the four VSDs from human Nav1.7, leaving the S4-S5 linker and PM of NavAb intact (Fig. 1H and fig. S3B). Because we were unable to record reliable voltage-activated Na^+ currents from these channels, we synthesized a suitable tritiated aryl sulfonamide compound, [^{3}H]GX-545, to enable affinity measurements utilizing radioligand binding assays. Membranes containing the VSD4-NavAb channel bound the [^{3}H]GX-545 radioligand with high affinity [dissociation constant (K_d) = 4 nM], whereas the VSD1, VSD2, and VSD3-NavAb chimeras showed low specific binding (K_d ≥30 nM), comparable to that of the parental NavAb channel (fig. S6). A strong linear correlation was observed between the VSD4-NavAb chimera and the native Nav1.7 channel when comparing the K_i's of 20 structurally diverse GX-series aryl sulfonamide compounds (Fig. 1I and tables S1 and S2). Notably, a strong correlation between functional channel inhibition and radioligand binding was also observed on the native Nav1.7 channel (Fig. 1J and tables S1 and S2), validating our use of [^{3}H]GX-545 binding to assess the degree to which the relevant receptor site is maintained within our chimeric constructs. We conclude that the high-affinity, Nav1.7-selective antagonist receptor site has been preserved within our VSD4-NavAb chimera.

The VSD4-NavAb chimera could be readily purified with a recovery yield of 5 mg/liter from insect cell culture, >1000-fold higher than expected for the native Nav1.7 channel; however, this VSD4-NavAb construct did not yield crystals. We hypothesized that removal of a minor crystal contact (fig. S5B) was precluding crystallization and engineered a channel in which a small intracellular portion of the NavAb VSD was reintroduced. The extracellular portion of VSD4 was left completely intact (Fig. 1H and fig. S3C), and the binding affinity of [^{3}H]GX-545 did not change (K_d = 4 nM; Fig. 1I and fig. S6), critically indicating that the protein engineering required to crystallize this human-bacterial VSD chimera does not perturb the GX-compound receptor site. This hybrid channel crystallized from a phosphatidylcholine-based bicelle system only in the presence of a potent aryl sulfonamide antagonist, and our best diffracting crystals were obtained in complex with GX-936. The GX-936-VSD4-NavAb structure was phased by molecular replacement using the available high-resolution model of NavAb (*12*) and refined to 3.53 Å resolution (table S3), with electron density maps of high quality (fig. S7). Crystal structures of VSD4-NavAb in complex with GX-629 (3.85 Å) and GX-674 (4.5 Å) have also been obtained (tables S1 and S3), and these are both highly similar to the GX-936 complex detailed below (fig. S8).

Structure of Nav1.7 VSD4-NavAb channels in a membrane environment

The VSD4-NavAb chimera displays the domain-swapped arrangement expected for a voltage-gated ion channel (*11*, *12*), and 22 phospholipids are seen bound to the channel, suggesting the maintenance of a native membrane-like environment (fig. S9, A and B). Crystal contacts are not observed between the Nav1.7-substituted portions of VSD4, implying that a relatively unconstrained conformation of the VSD has been captured (fig. S9, C and D). Despite replacing most of the NavAb VSD (Fig. 2A and fig. S3C), surface complementarity with the PM remains high, underscoring the noted sequence conservation between NavAb and human Nav channels (*12*, *13*). As seen in previous NavAb structures (*12*, *13*), the ion-conducting PM of the VSD4-NavAb chimeric channel is closed, consistent with a nonconductive or inactivated state.

During crystallographic refinement, strong residual electron density within the extracellular cleft of VSD4 allowed us to unambiguously position GX-936 (Fig. 2B). Unexpectedly, GX-936 is submerged below the membrane-aqueous interface, and a portion of the compound protrudes into the lipid bilayer (Fig. 2A). To corroborate the binding mode of GX-936, a bromide-substituted derivative (GX-629) was cocrystallized with VSD4-NavAb and analyzed through a single-wavelength anomalous

Downloaded from http://science.sciencemag.org/ on February 26, 2020

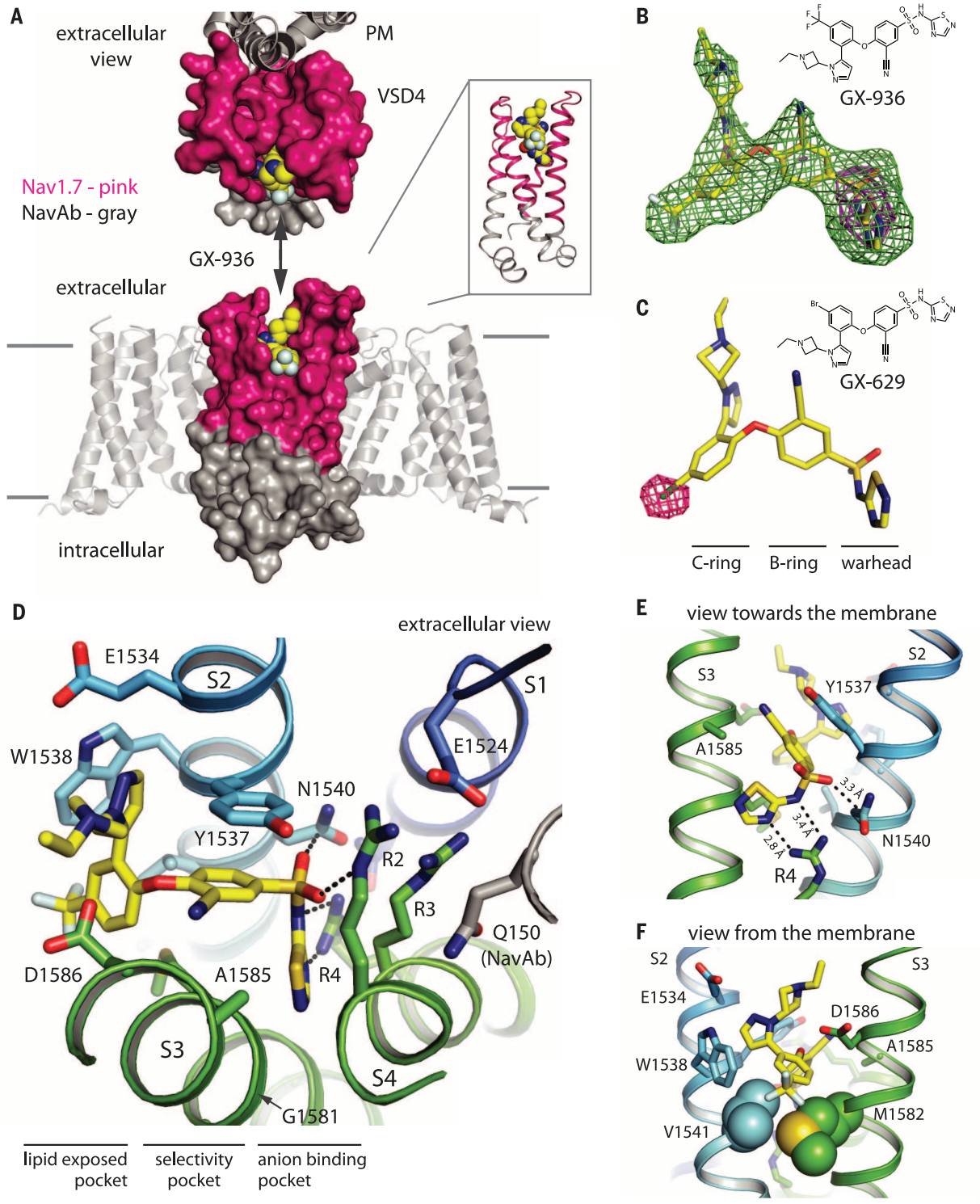

Fig. 2. Crystal structure of the Nav1.7 VSD4-NavAb channel in complex with GX-936. (**A**) A single VSD from the homotetrameric Nav1.7 VSD4-NavAb channel is shown in surface representation with GX-936 rendered in spheres. Grafted portions of human Nav1.7 VSD4 are highlighted in pink (see fig. S3C) and also shown in ribbon representation (inset). (**B**) $F_o - F_c$ map calculated to 3.53 Å before GX-936 was modeled, shown with the final refined coordinates of GX-936. Purple mesh contoured at 5.0 σ; green mesh contoured at 2.75 σ. (**C**) Anomalous difference Fourier map calculated to 3.85 Å from data at the Br absorption edge (λ = 0.9199 Å) contoured at 6 σ shown with the final refined coordinates of GX-629. (**D**) Nav1.7 VSD4 aryl sulfonamide receptor site is shown with select side chains rendered as sticks. Dashed lines represent ionic, hydrogen bonding, and electrostatic interactions between GX-936 and VSD4. Notably, Q150 from the NavAb PM S5 (gray) aligns with Q265 from DI S5 of human Nav1.7. (**E**) Side view highlighting key interactions with the GX-936 warhead. (**F**) V1541 and M1582 side chains forming the hydrophobic floor are shown in sphere representation; view is 180° relative to (E).

Downloaded from http://science.sciencemag.org/ on February 26, 2020

dispersion experiment (Fig. 2C). Similarly, a selenomethionine-incorporated protein crystal (4.35 Å) was used to landmark the five newly introduced methionine side chains from Nav1.7 VSD4 found around GX-936 (figs. S3C and S10 and table S3). Overall, these results unequivocally confirm the extracellular accessibility of the aryl sulfonamide binding site on Nav1.7 and the portability of the VSD4 receptor site onto NavAb.

Structural determinants of GX-936 binding to Nav1.7 VSD4-NavAb

Reminiscent of a Venus flytrap, the S1-S2 and S3-S4 helices from VSD4 form a clamshell-like structure that closes over GX-936 (Fig. 2, A and D). Human Nav1.7 residues completely engulf GX-936, whereas not a single NavAb side chain makes contact (Fig. 2A). This key result validates our experimental approach and allows us to define the structural determinants of this isoform-selective receptor site (movie 1). Upon inspection, the binding site of GX-936 and related aryl sulfonamides in Nav1.7 VSD4 can be divided into three regions: an anion-binding pocket, a selectivity pocket, and a lipid-exposed pocket (Figs. 2D and 3A).

The anionic warhead of GX-936 bisects VSD4 and sits deep within the extracellular cleft where the R4 gating charge (R1608) demarks the bottom of the anion-binding pocket (Figs. 2, D and E, and 3A). The guanidinium group of R4 engages the delocalized charge of the aryl sulfonamide thiadiazole headgroup through a bidentate salt bridge, which landmarks the interaction (Fig. 2, D and E). As anticipated by our electrophysiological studies, this pivotal gating charge–warhead interaction can rationalize the state dependence of GX-674 inhibition (Fig. 1, C, F, and G) because R4 will only be exposed to the extracellular side of the VSD when the membrane is sufficiently depolarized (*39*). The R3 gating charge (R1605) lines the front of the anion-binding pocket where its aliphatic portion makes van der Waals contact with GX-936 (Fig. 2D). R2 (R1602) engages the sulfonamide group of GX-936 from above through its ε-nitrogen, and the N1540 side chain (from S2) makes an electrostatic interaction with the adjacent sulfonamide oxygen (Fig. 2, D and E). All of the interactions that pin the anionic warhead into the anion-binding pocket arise from residues that are strictly conserved in human Nav channels (fig. S3A), suggesting that the determinants of Nav1.7 (as well as Nav1.2 and Nav1.6) molecular selectivity stem from elsewhere in the receptor site.

The selectivity pocket in the VSD4 receptor site is lined by the S2 and S3 helices, consistent with physiological studies that point toward the Y1537 and W1538 side chains as major determinants of isoform selectivity (Fig. 1E) (*31*). Y1537 (S2) forms a roof over the benzonitrile ring of GX-936 through a π-stacking interaction, while W1538 (S2) buttresses the pyrazole ring and walls off a portion of the selectivity pocket from the lipid bilayer (Fig. 2, D to F). Underneath GX-936, the V1541 (S2) and M1582 (S3) side chains form a hydrophobic floor that supports the trifluoromethylphenyl and benzonitrile rings through van der Waals contacts (Fig. 2F). Although E1534 (S2) and D1586 (S3) seem poised to make contact with the azetidine group of GX-936, neither side chain forms a direct interaction (≥3.9 Å; Fig. 2, D and F). By contrast, the small side chains of G1581 (S3) and A1585 (S3) provide good complementarity around GX-936 to allow closure of the VSD4 clamshell (Fig. 2, D and E). Consistent with sequence differences between Nav channel isoforms (fig. S3A), these first-shell S2 and S3 residues appear to present the molecular logic for binding specificity of the aryl sulfonamide antagonists to Nav1.7 (Fig. 1, D and E).

A lipid-exposed pocket is found in the VSD4 receptor site where the floor of the aryl sulfonamide-binding site sits 5 to 10 Å below the membrane-aqueous interface, judging by the positions of

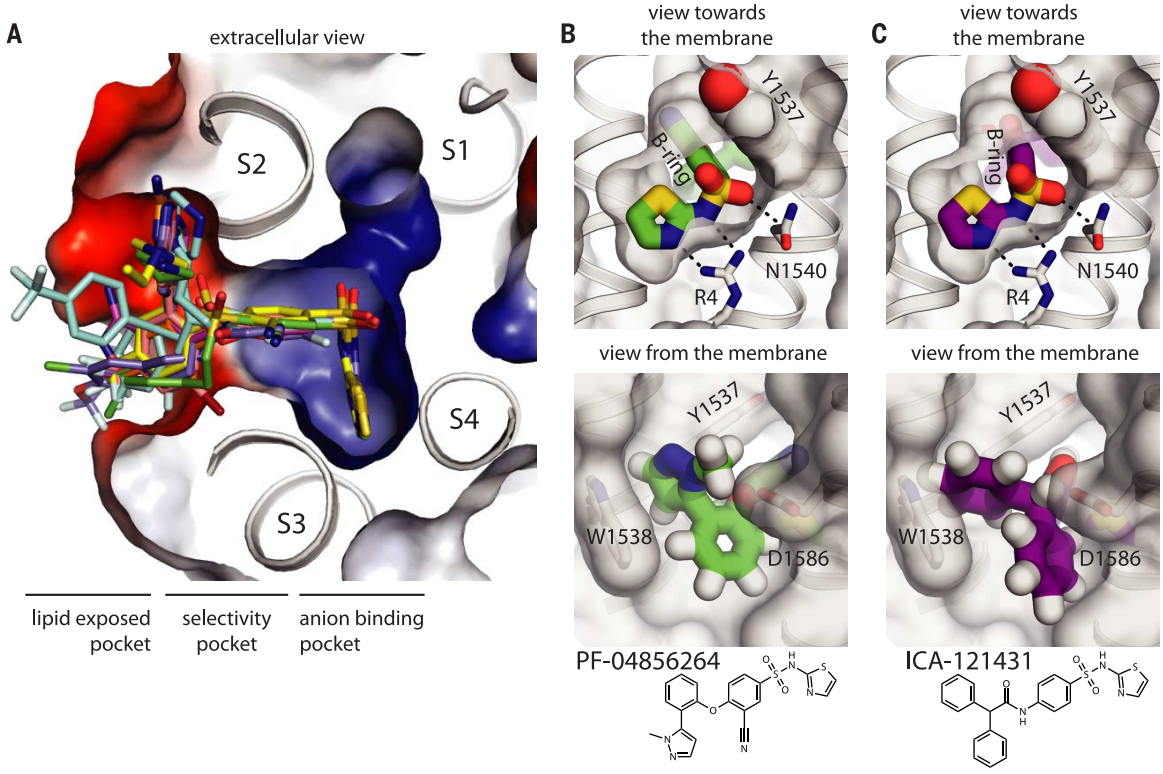

Fig. 3. Determinants of aryl sulfonamide isoform selectivity revealed by docking analyses in Nav1.7 VSD4-NavAb. (**A**) A selection of Nav channel inhibitors of the aryl sulfonamide class (fig. S11) are shown in their lowest-energy docked conformations superimposed onto the experimental coordinates of the GX-936-VSD4-NavAb crystal structure. GX-936 is shown in yellow sticks for reference. An electrostatic surface of the VSD4 binding site is shown: blue, basic regions; red, acidic regions; white, hydrophobic regions. Approximate boundaries of the lipid-exposed pocket, selectivity pocket, and anion-binding pocket are also indicated. The view is sectioned within the plane of the membrane, and bound lipids are omitted for clarity. (**B**) Docking of the Nav1.7 isoform-selective inhibitor, PF-04856264 (green stick representation), shows high correspondence to the position of GX-936 in the x-ray structure. (**C**) Docking of the Nav1.3/Nav1.1 isoform-selective inhibitor ICA-121431 (purple stick representation) indicates that formation of the favorable R4-warhead interaction leads to multiple unfavorable clashes with side chains in the Nav1.7 VSD4 receptor site (Y1537, W1538, and D1586) that are not conserved in Nav1.3/Nav1.1. For clarity, hydrogens are only represented in lower panels in order to best appreciate the fit (B) or steric clashes (C) of the respective compounds shown in this docking analysis.

Downloaded from http://science.sciencemag.org/ on February 26, 2020

annular phospholipids bound around the VSD4-NavAb channel (fig. S9, A and B). The trifluoromethylphenyl group of GX-936 points into the lipid-exposed pocket and makes limited protein contact (Fig. 2, A, D, and F, and Fig. 3A), presumably contributing little to the isoform selectivity profile of these antagonists. Direct exposure of GX-936 to the bilayer suggests a possible membrane-access mechanism for inhibitor binding to VSD4, which is intriguing because gating modifier toxins have also been shown to partition into the membrane (*44*–*48*). This result highlights an emerging concept that drugs may gain access to their binding sites on disparate channels or receptors through the membrane bilayer (*12*, *21*, *49*–*53*).

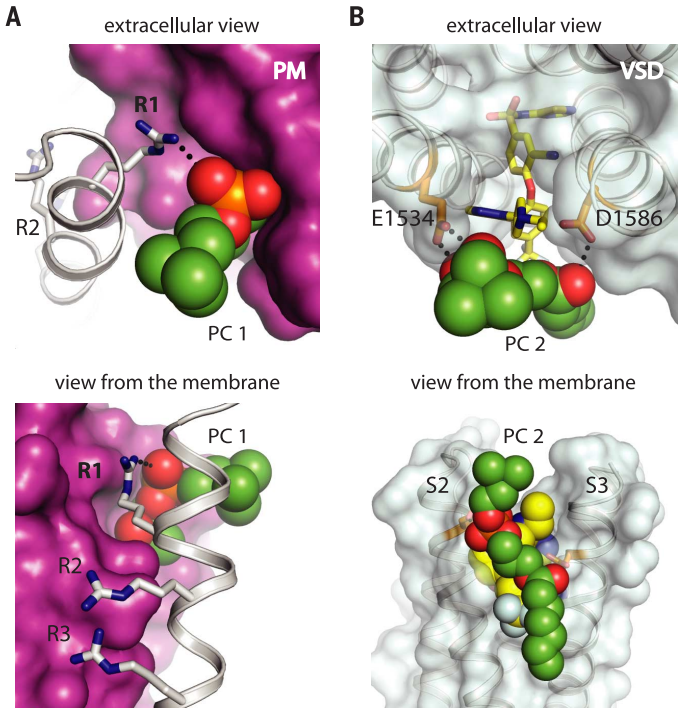

Fig. 4. Membrane phospholipids interact with Nav1.7 VSD4-NavAb and GX-936. (**A**) The R1 gating charge on S4 interacts with a phospholipid (PC1) phosphodiester group, as highlighted by a dashed line (~3.4 Å). The VSD4-NavAb channel was crystallized from a phosphatidylcholine (PC)–based bicelle system, and the extra electron density was well fit by a partial PC molecule (see Methods). (**B**) A partially modeled PC molecule (PC2) is observed beside the S2 and S3 helices. PC2 is coordinated to E1534 in all channel subunits in the asymmetric unit, and putatively coordinated to D1586 in two of the subunits within the asymmetric unit. Good surface complementarity between the PC2 and GX-936 is also observed. GX-936 is shown in yellow stick and sphere representation, and chain B of the VSD4-NavAb channel is shown in this panel.

VSD4 receptor site binding mode informs on selectivity

To explore the generality of the GX-936 binding mode beyond our GX-629 and GX-674 cocrystal structures (fig. S8 and tables S1 and S3), several inhibitors of the aryl sulfonamide class (*31*, *38*) were docked into the x-ray structure (Fig. 3 and fig. S11). For many compounds, including the Nav1.7 isoform-selective PF-04856264 (*31*), docking revealed a similar engagement of the anionic warhead with the R4 gating charge and a nearly perpendicular vector between the aryl sulfonamide moiety and the B-ring (Figs. 2D and 3, A and B, and fig. S11, A to I). These results highlight diverse substituents protruding into the lipid-exposed pocket (Fig. 3A) and suggest that a minimal pharmacophore may be required to engage Nav1.7. Our docking analysis supports the identification of two key selectivity motifs within VSD4 for Nav1.7-isoform–selective inhibitors like GX-674: YWxxV on S2 and GMxxA on S3 (Figs. 1, D and E, and 2, D to F, and fig. S3A). Accordingly, the Nav1.3-selective aryl sulfonamide ICA-121431 (*31*) could not be favorably docked into the Nav1.7 VSD4 receptor site, owing to clashes of this compound's B-ring and bulky biphenyl substitution on the C-ring with side chains from the YWxxV motif on S2 and D1586 on S3, respectively (Fig. 3C and fig. S11J).

Bound phospholipids surround the GX-936-VSD4-NavAb complex

The membrane bilayer has an increasingly recognized role in the function of voltage-gated ion channels, and the phosphodiester-containing headgroups of lipids are essential for voltage-dependent gating (*54*, *55*). We have assigned a

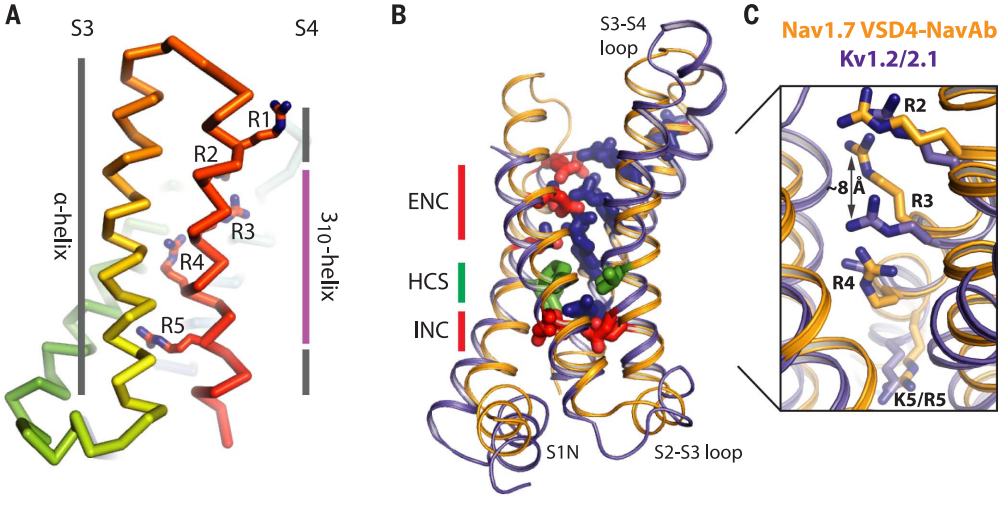

Fig. 5. GX-936 traps Nav1.7 VSD4 in an activated conformation. (**A**) Ribbon diagram representation of VSD4-NavAb highlights a 3_{10}-helical conformation extending across the middle of the S4 segment. By comparison, the S3 helix exists in an entirely α-helical conformation. GX-936 is omitted for clarity. (**B**) Superposition of Nav1.7 VSD4-NavAb (orange) with the rat Kv1.2/2.1 channel VSD (purple; PDB 2R9R) highlights their overall structural likeness and conformational similarity. Gating charges and residues from the conserved extracellular negative charge cluster (ENC), hydrophobic constriction site (HCS), and intracellular negative charge cluster (INC) regions are shown in stick representations and colored purple, red, green, and red, respectively. GX-936 in VSD4 and the S1-S2 loop in Kv1.2/2.1 are omitted for clarity. (**C**) Zoom-in view highlights the close spatial correspondence between gating charges in VSD4-NavAb (orange) and Kv1.2/2.1 (purple).

Downloaded from http://science.sciencemag.org/ on February 26, 2020

number of electron densities within the GX-936-VSD4-NavAb structure as phosphatidylcholine (PC) molecules, in part, because this channel was crystallized in the presence of high concentrations of PC (see Methods). We find that the outermost R1 gating charge (R1599) in VSD4 forms an ion-pair interaction with the phosphodiester group of a glycerophospholipid (PC 1) that is nestled between the VSD and PM (Fig. 4A, movie 2, and fig. S9E). Although direct contact between an S4 arginine and a lipid headgroup has not been seen in previous Kv or bacterial Nav channel structures (*10*–*14*), our crystallographic observations clearly support the view that gating charges can make compensating interactions with phospholipids to stabilize different gating states of the VSD and channel (*54*–*56*).

The precise composition of the membrane bilayer also influences Nav channel pharmacology in important ways. Some gating modifier toxins are known to partition into lipid membranes (*44*–*48*), and early reconstitution studies with purified Nav channels established that distinct lipid mixtures are required to recover α-scorpion toxin binding (*57*). Enzymatic removal of sphingomyelin headgroups can also modulate the binding of gating modifier toxins through the disruption of a postulated ternary lipid-toxin-channel complex (*47*). However, it remains unknown if these reports of pharmacological modulation stem from direct or indirect lipid interactions with Nav channels. Here, we find strong electron density, unseen in previous NavAb structures (*12*, *13*), attributed to a bound phospholipid (PC 2) buttressing the GX-936 binding site (Fig. 4B, movie 3, and fig. S9F). This peripherally bound lipid covers ~200 Å^2 of GX-936 surface and forms specific interactions with side chains from the S2 and S3 helices (E1534 and D1586, respectively; Fig. 4B and movie 3). Our experimental observation of a lipid-antagonist-VSD4 ternary complex raises the distinct possibility that membrane lipids can directly modulate the structure and character of the VSD4 receptor site of Nav1.7 within cells.

Small-molecule gating modifiers trap VSD4 in an activated state

Unlike α-scorpion and sea anemone toxins that are known to impair VSD4 activation (*28*, *41*), our functional and structural studies suggest that compounds like GX-674 and GX-936 bind to the activated state of VSD4 (Fig. 1, C, F, and G, and fig. S8). When VSD4 is trapped in this state, four gating charges (R1–R4) are exposed to the extracellular cleft of VSD4, whereas R5 (R1611) remains engaged with the intracellular negative charge cluster (Fig. 5, A and B). A 3_{10}-helical

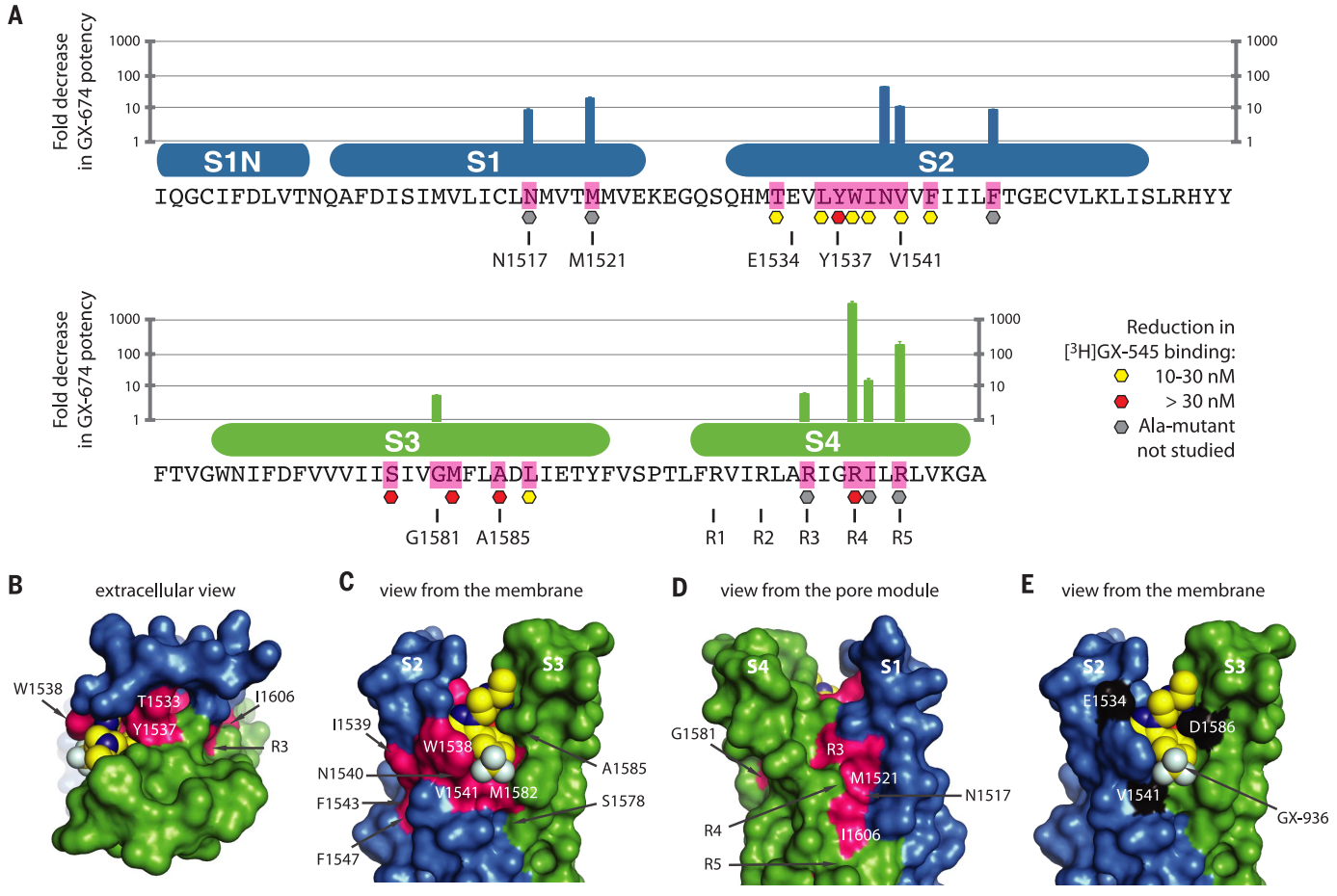

Fig. 6. Structural determinants of aryl sulfonamide binding and selectivity in Nav1.7 VSD4. (**A**) The native Nav1.7 VSD4 sequence is shown with data from a scanning mutagenesis study measured by electrophysiology using GX-674 on full-length human Nav1.7 channels (top, bar graph) or radioligand binding to chimeric VSD4-NavAb channels using [^{3}H]GX-545 (below, hexagonal symbols). Fold-reduction in GX-674 potency is measured relative to wild-type Nav1.7. A1585 was mutated to Phe for the [^{3}H]GX-545 study; and R3 was mutated to Gln for the GX-674 study (because R3A channels failed to generate currents sufficient for study). See Methods for experimental details and fig. S14 to S18 for the full extent of mutations studied. For electrophysiology data: $n \geq 3$; error bars indicate SEM. (**B** to **D**) Residue positions affecting IC_{50} and/or K_d from site-directed mutational scans of native Nav1.7 and chimeric VSD4-NavAb channels, respectively, are highlighted in pink and mapped onto a surface representation of VSD4-NavAb. The S1-S2 region is colored blue, the S3-S4 region is colored green, and GX-936 is shown in yellow sphere representation. (**E**) Three first-shell residues within 5 Å of contact of GX-936 that are not conserved among Nav1.7, Nav1.2, and Nav1.6 channel isoforms are highlighted in black. The similar potencies of GX-674 on the Nav1.7, Nav1.2, and Nav1.6 channel isoforms (Fig. 1D) suggest that these three side-chain positions might be exploited in future structure-based drug design efforts. In Nav1.7, the three residues in question are E1534, V1541, and D1586; whereas the equivalents in Nav1.2 are Asn, Leu, and Glu; and in Nav1.6 are Asn, Leu, and Asp (see fig. S3A).

Downloaded from http://science.sciencemag.org/ on February 26, 2020

conformation in S4 spans across R2–R5 (Fig. 5A), allowing these gating charges to form an interlaced interaction network that participates in closure of the VSD4 clamshell around GX-936–like compounds (movie 2).

The presence of a cocrystallized state-dependent inhibitor pharmacologically stabilizes an activated state of the VSD4 structure. Therefore, the pronounced resemblance between inhibitor-bound VSD4 and rat Kv1.2 VSD (*11*), where the spatial correspondence between equivalent gating charges is <1 Å, suggests a ubiquitous pathway for S4 activation (Fig. 5, B and C, and movie 4). Only R3 in VSD4 is laterally displaced to accommodate binding of the GX-936 warhead to R4 (Fig. 5C). Despite limited sequence identity (fig. S3D) or the presence of a small-molecule antagonist (Fig. 2), these structural observations imply that a shared conformation exists in the activated state of mammalian Nav and Kv VSDs (*58*) (movie 4).

Until now, it has been unclear to what extent the bacterial Nav channel VSDs resemble the four mammalian Nav channel VSDs, VSD1–4, because these mammalian VSDs have distinct sequences with unique functions and pharmacology (*16*, *37*, *40*). Superposition of VSD4-NavAb coordinates onto the parental VSD from NavAb (*12*) demonstrates that mammalian and bacterial S1–S4 domains share very similar structures in the activated state (fig. S12). Our VSD4-NavAb structure further reveals an elongation of S3 by three helical turns and other vertebrate-specific elaborations (fig. S12 and movie 4), providing more accurate models of the four mammalian VSDs to interpret physiological data (*59*) and guide drug discovery (fig. S13). Because the VSD4-NavAb protein that we engineered for crystallography is actually a hybrid of human and bacterial components (Fig. 2A and fig. S3), the chimeric nature of this construct confirms the likeness of mammalian and bacterial VSDs since high-affinity radioligand binding is maintained (fig. S6), rather than destroyed.

Mutational analyses of the Nav1.7 VSD4 receptor site

To dissect contributions of aryl sulfonamide binding to the VSD4 receptor site, we performed scanning mutagenesis on the human Nav1.7 channel (figs. S14 to S16). Within the anion-binding pocket, N1540A (S2) and R4A (S4) mutations had the largest effect, reducing GX-674 potency by a factor of 43 and 3000, respectively (Fig. 6, A to D). R3Q (in place of R3A) and R5A reduced GX-674 potency by a factor of 6 and 170, indicating that these gating charges may stabilize the local structure of the S4 (Figs. 5A and 6, A to D, and fig. S16). R1A and R2A did not significantly affect GX-674 potency (fig. S16), suggesting that the observed R1-lipid and R2-sulfonamide oxygen interactions contribute minimally (~3.4 Å; Figs. 2D and 4A). Alanine scanning further revealed 9- to 20-fold effects on GX-674 inhibition for residues that directly or indirectly encase R4 (Fig. 6, A to D, and figs. S14 and S17), underscoring the importance of precisely positioning the R4 side chain. Mutation of R4 to lysine (R4K) decreased GX-674 potency by a factor of 675 (fig. S16), further highlighting the bidentate interaction seen between R4 and the aryl sulfonamide thiadiazole moiety (Fig. 2E). Overall, the potency of Nav1.7 inhibition by this class of molecules is dominated by the R4 gating charge interaction, in line with the voltage dependence required to expose this side chain into the extracellular cleft to engage the anionic warhead (Figs. 1, C, F, and G, and 2, D to F).

To better understand the selectivity pocket within the VSD4 receptor site, we used GX-674 and [^{3}H]GX-545 to assay human Nav1.7 or VSD4-NavAb channels, respectively. V1541A (S2; YWxx**V**) and M1582A (S3; G**M**xxA) mutations decreased antagonist affinity, highlighting the hydrophobic floor in forming an optimal receptor site and pointing to side-chain differences among Nav channel isoforms (Fig. 6, A to E, and fig. S3A). G1581A and A1585F mutations within the S3 **G**Mxx**A** selectivity motif reduced antagonist potency, owing to the introduction of steric hindrance (Fig. 6, A to D); and because equivalent residues in VSD1-3 are larger than alanine, this result can explain the selective targeting of VSD4 by the aryl sulfonamides (figs. S3A and S13). Inhibitor potencies were substantially decreased in both human Nav1.7 and VSD4-NavAb channels when Y1537 and W1538 were simultaneously mutated to their Nav1.1 or Nav1.3 equivalents Y1537S/W1538R (Figs. 1E and 6, A to D, and fig. S18), solidifying the importance of the S2 **YW**xxV motif in determining isoform selectivity of the aryl sulfonamide antagonists. Interestingly, the single mutation Y1537S (as well as Y1537A) increased GX-674 potency and increased the on-rate and off-rate of GX-674 inhibition (fig. S18), suggesting that the bulky tyrosine side chain may restrict access to the binding pocket. Furthermore, the mutation W1538R did not by itself alter GX-674 potency, suggesting that a complex interaction between Y1537, W1538, and GX-674 exists to establish isoform selectivity (fig. S18, A and B).

Mapping the mutations that have effects on antagonist affinity (fig. S17) in combination with VSD4 homology modeling will guide isoform-selective Nav channel inhibitor design efforts. The S2 selectivity motif in Nav1.7 is YWxx**V**, but YWxxL in Nav1.2 and Nav1.6 (Fig. 1E), which together with nearby side-chain differences (Fig. 6E and fig. S3A) provides an opportunity for the development of truly Nav1.7-selective inhibitors. Alternatively, the design of "central nervous system (CNS)–sparing" aryl sulfonamides that target Nav1.7 with only limited isoform-selectivity against Nav1.2 and Nav1.6 (Fig. 1D) might still enable safe and effective treatment for pain, because the dose-limiting side effects of blockers that lack molecular selectivity (*60*) likely involve the Nav1.2 and Nav1.6 channels, which are abundantly expressed in the CNS (*4*).

Discussion

Nav channel inhibitors have traditionally been classified as either functionally selective, where binding is modified by channel gating (e.g., local anesthetics), or molecularly selective, where potency differs among Nav channel isoforms with little interaction from gating (e.g., tetrodotoxin). All clinically used Nav channel inhibitors are functionally selective, where their time- and state-dependence of block favors patterns of electrical activity seen in pathological conditions. Our structural studies define the mechanism of action of a new class of compounds (*31*, *38*) that possess both functional and molecular selectivity, a phenomenon previously unknown among small-molecule ligands of the Nav channel family (*32*–*34*). Inhibition by the aryl sulfonamides is exquisitely sensitive to channel activation, which derives from the requisite movement of the R4 gating charge into the extracellular cleft of VSD4 to form pivotal contacts with the antagonist's anionic warhead. The VSD4 location of the binding site on Nav channels is likely mechanistically meaningful because charge movement of S4 in VSD4 is necessary and sufficient for fast inactivation (*40*). Therefore, by targeting and immobilizing the S4 helix of VSD4, the R4-warhead interaction underlies the voltage-sensor trapping mechanism of Nav channel inhibition by these small-molecule gating modifier antagonists.

We have exploited a bacterial Nav channel to obtain crystal structures of human Nav1.7 VSD4 in complex with potent and isoform-selective small-molecule inhibitors. Our structures reveal the details of a remarkable Nav channel VSD4 receptor site, where residues conserved in all Nav channels are required for high-affinity binding, and side chains from the S2 and S3 helices are key determinants of isoform selectivity. In addition to establishing a close structural relationship between prokaryotic and eukaryotic VSDs, a potential membrane access pathway for small-molecule gating modifiers and roles for phospholipids in modulating Nav channel function have also been noted. Indeed, we have observed a unique phospholipid-antagonist-VSD4 tripartite interaction that may expand the importance of the lipid bilayer in ion channel biology and pharmacology. Ultimately, we anticipate that our new crystallization strategy will form the basis for drug design efforts aimed at other voltage-gated ion channels (*32*–*34*) and hope that the Nav1.7 structures reported here will accelerate the development of superior treatments for pain.

REFERENCES AND NOTES

1. B. Hille, *Ion Channels of Excitable Membranes* (Sinauer, Sunderland, MA, ed. 3, 2001).
2. W. A. Catterall, Structure and function of voltage-gated ion channels. *Annu. Rev. Biochem.* **64**, 493–531 (1995). doi: 10.1146/annurev.bi.64.070195.002425; pmid: 7574491
3. J. Payandeh, D. L. Minor Jr., Bacterial voltage-gated sodium channels (BacNa(V)s) from the soil, sea, and salt lakes enlighten molecular mechanisms of electrical signaling and pharmacology in the brain and heart. *J. Mol. Biol.* **427**, 3–30 (2015). doi: 10.1016/j.jmb.2014.08.010; pmid: 25158094
4. W. A. Catterall, A. L. Goldin, S. G. Waxman, International Union of Pharmacology, International Union of Pharmacology. XLVII. Nomenclature and structure-function relationships of voltage-gated sodium channels. *Pharmacol. Rev.* **57**, 397–409 (2005). doi: 10.1124/pr.57.4.4; pmid: 16382098
5. S. D. Dib-Hajj, Y. Yang, J. A. Black, S. G. Waxman, The Na(V)1.7 sodium channel: From molecule to man. *Nat. Rev. Neurosci.* **14**, 49–62 (2013). doi: 10.1038/nrn3404; pmid: 23232607

Downloaded from http://science.sciencemag.org/ on February 26, 2020

6. C. R. Fertleman *et al*., SCN9A mutations in paroxysmal extreme pain disorder: Allelic variants underlie distinct channel defects and phenotypes. *Neuron* **52**, 767–774 (2006). doi: 10.1016/j.neuron.2006.10.006; pmid: 17145499
7. Y. Yang *et al*., Mutations in SCN9A, encoding a sodium channel alpha subunit, in patients with primary erythermalgia. *J. Med. Genet.* **41**, 171–174 (2004). doi: 10.1136/jmg.2003.012153; pmid: 14985375
8. J. J. Cox *et al*., An SCN9A channelopathy causes congenital inability to experience pain. *Nature* **444**, 894–898 (2006). doi: 10.1038/nature05413; pmid: 17167479
9. Y. P. Goldberg *et al*., Loss-of-function mutations in the Nav1.7 gene underlie congenital indifference to pain in multiple human populations. *Clin. Genet.* **71**, 311–319 (2007). doi: 10.1111/j.1399-0004.2007.00790.x; pmid: 17470132
10. Y. Jiang *et al*., X-ray structure of a voltage-dependent K^+ channel. *Nature* **423**, 33–41 (2003). doi: 10.1038/nature01580; pmid: 12721618
11. S. B. Long, X. Tao, E. B. Campbell, R. MacKinnon, Atomic structure of a voltage-dependent K^+ channel in a lipid membrane-like environment. *Nature* **450**, 376–382 (2007). doi: 10.1038/nature06265; pmid: 18004376
12. J. Payandeh, T. Scheuer, N. Zheng, W. A. Catterall, The crystal structure of a voltage-gated sodium channel. *Nature* **475**, 353–358 (2011). doi: 10.1038/nature10238; pmid: 21743477
13. J. Payandeh, T. M. Gamal El-Din, T. Scheuer, N. Zheng, W. A. Catterall, Crystal structure of a voltage-gated sodium channel in two potentially inactivated states. *Nature* **486**, 135–139 (2012). pmid: 22678296
14. X. Zhang *et al*., Crystal structure of an orthologue of the NaChBac voltage-gated sodium channel. *Nature* **486**, 130–134 (2012). pmid: 22678295
15. W. Stühmer *et al*., Structural parts involved in activation and inactivation of the sodium channel. *Nature* **339**, 597–603 (1989). doi: 10.1038/339597a0; pmid: 2543931
16. B. Chanda, F. Bezanilla, Tracking voltage-dependent conformational changes in skeletal muscle sodium channel during activation. *J. Gen. Physiol.* **120**, 629–645 (2002). doi: 10.1085/jgp.20028679; pmid: 12407076
17. B. Hille, The receptor for tetrodotoxin and saxitoxin. A structural hypothesis. *Biophys. J.* **15**, 615–619 (1975). doi: 10.1016/S0006-3495(75)85842-5; pmid: 1148362
18. G. R. Strichartz, The inhibition of sodium currents in myelinated nerve by quaternary derivatives of lidocaine. *J. Gen. Physiol.* **62**, 37–57 (1973). doi: 10.1085/jgp.62.1.37; pmid: 4541340
19. H. A. Fozzard, P. J. Lee, G. M. Lipkind, Mechanism of local anesthetic drug action on voltage-gated sodium channels. *Curr. Pharm. Des.* **11**, 2671–2686 (2005). doi: 10.2174/1381612054546833; pmid: 16101448
20. C. Bagnéris *et al*., Prokaryotic NavMs channel as a structural and functional model for eukaryotic sodium channel antagonism. *Proc. Natl. Acad. Sci. U.S.A.* **111**, 8428–8433 (2014). doi: 10.1073/pnas.1406855111; pmid: 24850863
21. B. Hille, Local anesthetics: Hydrophilic and hydrophobic pathways for the drug-receptor reaction. *J. Gen. Physiol.* **69**, 497–515 (1977). doi: 10.1085/jgp.69.4.497; pmid: 300786
22. B. P. Bean, Nitrendipine block of cardiac calcium channels: High-affinity binding to the inactivated state. *Proc. Natl. Acad. Sci. U.S.A.* **81**, 6388–6392 (1984). doi: 10.1073/pnas.81.20.6388; pmid: 6093100
23. M. C. Sanguinetti, R. S. Kass, Regulation of cardiac calcium channel current and contractile activity by the dihydropyridine Bay K 8644 is voltage-dependent. *J. Mol. Cell. Cardiol.* **16**, 667–670 (1984). doi: 10.1016/S0022-2828(84)80631-8; pmid: 6206231
24. M. J. Wilson *et al*., μ-Conotoxins that differentially block sodium channels $Na_v1.1$ through 1.8 identify those responsible for action potentials in sciatic nerve. *Proc. Natl. Acad. Sci. U.S.A.* **108**, 10302–10307 (2011). doi: 10.1073/pnas.1107027108; pmid: 21652775
25. O. Knapp, J. R. McArthur, D. J. Adams, Conotoxins targeting neuronal voltage-gated sodium channel subtypes: Potential analgesics? *Toxins (Basel)* **4**, 1236–1260 (2012). doi: 10.3390/toxins4111236; pmid: 23202314
26. S. England, D. Rawson, Isoform-selective voltage-gated Na^+ channel modulators as next-generation analgesics. *Future Med. Chem.* **2**, 775–790 (2010). pmid: 21426202
27. C. J. Cohen, Targeting voltage-gated sodium channels for treating neuropathic and inflammatory pain. *Curr. Pharm. Biotechnol.* **12**, 1715–1719 (2011). doi: 10.2174/138920111798357249; pmid: 21466442
28. F. Bosmans, K. J. Swartz, Targeting voltage sensors in sodium channels with spider toxins. *Trends Pharmacol. Sci.* **31**, 175–182 (2010). doi: 10.1016/j.tips.2009.12.007; pmid: 20097434
29. M. de Lera Ruiz, R. L. Kraus, Voltage-Gated Sodium Channels: Structure, Function, Pharmacology, and Clinical Indications. *J. Med. Chem.* **58**, 7093–7118 (2015). doi: 10.1021/jm501981g; pmid: 25927480
30. J. K. Murray *et al*., Engineering potent and selective analogues of GpTx-1, a tarantula venom peptide antagonist of the $Na_v1.7$ sodium channel. *J. Med. Chem.* **58**, 2299–2314 (2015). doi: 10.1021/jm501765v; pmid: 25658507
31. K. McCormack *et al*., Voltage sensor interaction site for selective small molecule inhibitors of voltage-gated sodium channels. *Proc. Natl. Acad. Sci. U.S.A.* **110**, E2724–E2732 (2013). doi: 10.1073/pnas.1220844110; pmid: 23818614
32. K. Padilla, A. D. Wickenden, A. C. Gerlach, K. McCormack, The KCNQ2/3 selective channel opener ICA-27243 binds to a novel voltage-sensor domain site. *Neurosci. Lett.* **465**, 138–142 (2009). doi: 10.1016/j.neulet.2009.08.071; pmid: 19733209
33. A. Peretz *et al*., Targeting the voltage sensor of Kv7.2 voltage-gated K^+ channels with a new gating-modifier. *Proc. Natl. Acad. Sci. U.S.A.* **107**, 15637–15642 (2010). doi: 10.1073/pnas.0911294107; pmid: 20713704
34. N. E. Ottosson *et al*., Resin-acid derivatives as potent electrostatic openers of voltage-gated K channels and suppressors of neuronal excitability. *Sci. Rep.* **5**, 13278 (2015). doi: 10.1038/srep13278; pmid: 26299574
35. Z. Lu, A. M. Klem, Y. Ramu, Ion conduction pore is conserved among potassium channels. *Nature* **413**, 809–813 (2001). doi: 10.1038/35101535; pmid: 11677598
36. A. A. Alabi, M. I. Bahamonde, H. J. Jung, J. I. Kim, K. J. Swartz, Portability of paddle motif function and pharmacology in voltage sensors. *Nature* **450**, 370–375 (2007). doi: 10.1038/nature06266; pmid: 18004375
37. F. Bosmans, M. F. Martin-Eauclaire, K. J. Swartz, Deconstructing voltage sensor function and pharmacology in sodium channels. *Nature* **456**, 202–208 (2008). doi: 10.1038/nature07473; pmid: 19005548
38. U. Norinder, M. E. Ek, QSAR investigation of NaV1.7 active compounds using the SVM/Signature approach and the Bioclipse Modeling platform. *Bioorg. Med. Chem. Lett.* **23**, 261–263 (2013). doi: 10.1016/j.bmcl.2012.10.102; pmid: 23177785
39. N. Yang, A. L. George Jr., R. Horn, Molecular basis of charge movement in voltage-gated sodium channels. *Neuron* **16**, 113–122 (1996). doi: 10.1016/S0896-6273(00)80028-8; pmid: 8562074
40. D. L. Capes, M. P. Goldschen-Ohm, M. Arcisio-Miranda, F. Bezanilla, B. Chanda, Domain IV voltage-sensor movement is both sufficient and rate limiting for fast inactivation in sodium channels. *J. Gen. Physiol.* **142**, 101–112 (2013). doi: 10.1085/jgp.201310998; pmid: 23858005
41. F. V. Campos, B. Chanda, P. S. Beirão, F. Bezanilla, Alpha-scorpion toxin impairs a conformational change that leads to fast inactivation of muscle sodium channels. *J. Gen. Physiol.* **132**, 251–263 (2008). pmid: 18663133
42. R. E. Middleton *et al*., Two tarantula peptides inhibit activation of multiple sodium channels. *Biochemistry* **41**, 14734–14747 (2002). doi: 10.1021/bi026546a; pmid: 12475222
43. K. Takeshita *et al*., X-ray crystal structure of voltage-gated proton channel. *Nat. Struct. Mol. Biol.* **21**, 352–357 (2014). doi: 10.1038/nsmb.2783; pmid: 24584463
44. S. Y. Lee, R. MacKinnon, A membrane-access mechanism of ion channel inhibition by voltage sensor toxins from spider venom. *Nature* **430**, 232–235 (2004). doi: 10.1038/nature02632; pmid: 15241419
45. J. J. Smith, S. Alphy, A. L. Seibert, K. M. Blumenthal, Differential phospholipid binding by site 3 and site 4 toxins. Implications for structural variability between voltage-sensitive sodium channel domains. *J. Biol. Chem.* **280**, 11127–11133 (2005). doi: 10.1074/jbc.M412552200; pmid: 15632158
46. M. Milescu *et al*., Tarantula toxins interact with voltage sensors within lipid membranes. *J. Gen. Physiol.* **130**, 497–511 (2007). doi: 10.1085/jgp.200709869; pmid: 17938232
47. M. Milescu *et al*., Interactions between lipids and voltage sensor paddles detected with tarantula toxins. *Nat. Struct. Mol. Biol.* **16**, 1080–1085 (2009). doi: 10.1038/nsmb.1679; pmid: 19783984
48. K. Gupta *et al*., Tarantula toxins use common surfaces for interacting with Kv and ASIC ion channels. *eLife* **4**, e06774 (2015). doi: 10.7554/eLife.06774; pmid: 25948544
49. S. D. Silberberg, M. Li, K. J. Swartz, Ivermectin interaction with transmembrane helices reveals widespread rearrangements during opening of P2X receptor channels. *Neuron* **54**, 263–274 (2007). doi: 10.1016/j.neuron.2007.03.020; pmid: 17442247
50. R. E. Hibbs, E. Gouaux, Principles of activation and permeation in an anion-selective Cys-loop receptor. *Nature* **474**, 54–60 (2011). doi: 10.1038/nature10139; pmid: 21572436
51. H. Nury *et al*., X-ray structures of general anaesthetics bound to a pentameric ligand-gated ion channel. *Nature* **469**, 428–431 (2011). doi: 10.1038/nature09647; pmid: 21248852
52. M. A. Hanson *et al*., Crystal structure of a lipid G protein-coupled receptor. *Science* **335**, 851–855 (2012). doi: 10.1126/science.1215904; pmid: 22344443
53. Y. Y. Dong *et al*., K2P channel gating mechanisms revealed by structures of TREK-2 and a complex with Prozac. *Science* **347**, 1256–1259 (2015). doi: 10.1126/science.1261512; pmid: 25766236
54. D. Schmidt, Q. X. Jiang, R. MacKinnon, Phospholipids and the origin of cationic gating charges in voltage sensors. *Nature* **444**, 775–779 (2006). doi: 10.1038/nature05416; pmid: 17136096
55. Y. Xu, Y. Ramu, Z. Lu, Removal of phospho-head groups of membrane lipids immobilizes voltage sensors of K^+ channels. *Nature* **451**, 826–829 (2008). doi: 10.1038/nature06618; pmid: 18273018
56. R. K. Hite, J. A. Butterwick, R. MacKinnon, Phosphatidic acid modulation of Kv channel voltage sensor function. *eLife* **3**, e04366 (2014). doi: 10.7554/eLife.04366; pmid: 25285449
57. D. J. Feller, J. A. Talvenheimo, W. A. Catterall, The sodium channel from rat brain. Reconstitution of voltage-dependent scorpion toxin binding in vesicles of defined lipid composition. *J. Biol. Chem.* **260**, 11542–11547 (1985). pmid: 2413014
58. X. Tao, A. Lee, W. Limapichat, D. A. Dougherty, R. MacKinnon, A gating charge transfer center in voltage sensors. *Science* **328**, 67–73 (2010). doi: 10.1126/science.1185954; pmid: 20360102
59. S. A. Pless *et al*., Asymmetric functional contributions of acidic and aromatic side chains in sodium channel voltage-sensor domains. *J. Gen. Physiol.* **143**, 645–656 (2014). doi: 10.1085/jgp.201311036; pmid: 24778431
60. E. Kalso, M. R. Tramèr, H. J. McQuay, R. A. Moore, Systemic local-anaesthetic-type drugs in chronic pain: A systematic review. *Eur. J. Pain* **2**, 3–14 (1998). doi: 10.1016/S1090-3801(98)90041-6; pmid: 10700296

ACKNOWLEDGMENTS

We thank our colleagues in the Structural Biology, Biology, Neuroscience, Discovery Chemistry, Biochemical and Cellular Pharmacology, and Chemistry Departments at Genentech and Xenon for project support. We especially appreciate the efforts of P. Bichler, C. Eigenbrot, W. Wang, P. Lupardus, B. Sellers, R. Mayer, J. Kiefer, T. Maurer, and S. Hymowitz in their support of this project. We acknowledge the European Synchrotron Radiation Facility for provision of synchrotron radiation facilities and thank S. Monac for assistance in using beamline ID29. A portion of this work was carried out with the support of the Diamond Light Source beamline I24, and we thank J. Waterman and A. Dias for assistance. Use of the Stanford Synchrotron Radiation Lightsource SSRL 12-12 at Stanford Linear Accelerator Center National Accelerator Laboratory is supported by the U.S. Department of Energy (DOE), DOE Office of Biological and Environmental Research, National Institutes of Health, and National Institute of General Medical Sciences. The contents of this publication are the responsibility of the authors and do not necessarily represent the views of NIH or National Institute of General Medical Sciences. Reagents used in this study are available under a materials transfer agreement with Genentech. T. Focken is inventor on patent application WO 2013/064984 that covers compounds GX-674, cmp6 (fig. S11), GX-0328, GX-3340, GX-4377, GX-4195, GX-4197, GX-4251, GX-4309, GX-4338, and GX-4375. Xenon Pharmaceuticals additionally holds patent application WO 2013/064983 that covers GX-4314. Structure factors and coordinates for the GX-936-VSD4-NavAb structure have been deposited in the Protein Data Bank with the accession code 5EK0. All authors are employees of Genentech Inc. or Xenon Pharmaceuticals Inc.

SUPPLEMENTARY MATERIALS

www.sciencemag.org/content/350/6267/aac5464/suppl/DC1
Materials and Methods
Figs. S1 to S18
Tables S1 to S3
Chemical synthesis of GX-545, GX-629, GX-674, and GX-936.

10 May 2015; accepted 29 October 2015
10.1126/science.aac5464

Downloaded from http://science.sciencemag.org/ on February 26, 2020

Science

Structural basis of Nav1.7 inhibition by an isoform-selective small-molecule antagonist

Shivani Ahuja, Susmith Mukund, Lunbin Deng, Kuldip Khakh, Elaine Chang, Hoangdung Ho, Stephanie Shriver, Clint Young, Sophia Lin, J. P. Johnson Jr., Ping Wu, Jun Li, Mary Coons, Christine Tam, Bobby Brillantes, Honorio Sampang, Kyle Mortara, Krista K. Bowman, Kevin R. Clark, Alberto Estevez, Zhiwei Xie, Henry Verschoof, Michael Grimwood, Christoph Dehnhardt, Jean-Christophe Andrez, Thilo Focken, Daniel P. Sutherlin, Brian S. Safina, Melissa A. Starovasnik, Daniel F. Ortwine, Yvonne Franke, Charles J. Cohen, David H. Hackos, Christopher M. Koth and Jian Payandeh

Science **350** (6267), aac5464.
DOI: 10.1126/science.aac5464

A channel involved in pain perception

Voltage-gated sodium (Nav) channels propagate electrical signals in muscle cells and neurons. In humans, Nav1.7 plays a key role in pain perception. It is challenging to target a particular Nav isoform; however, arylsulfonamide antagonists selective for Nav1.7 have been reported recently. Ahuja *et al.* characterized the binding of these small molecules to human Nav channels. To further investigate the mechanism, they engineered a bacterial Nav channel to contain features of the Nav1.7 voltage-sensing domain that is targeted by the antagonist and determined the crystal structure of the chimera bound to an inhibitor. The structure gives insight into the mechanism of voltage sensing and will enable the design of more-selective Nav channel antagonists.

Science, this issue p. 10.1126/science.aac5464

ARTICLE TOOLS http://science.sciencemag.org/content/350/6267/aac5464

SUPPLEMENTARY MATERIALS http://science.sciencemag.org/content/suppl/2015/12/16/350.6267.aac5464.DC1

RELATED CONTENT http://stke.sciencemag.org/content/sigtrans/7/352/ra109.full
http://stke.sciencemag.org/content/sigtrans/8/399/ra103.full

REFERENCES This article cites 59 articles, 19 of which you can access for free
http://science.sciencemag.org/content/350/6267/aac5464#BIBL

PERMISSIONS http://www.sciencemag.org/help/reprints-and-permissions

Use of this article is subject to the Terms of Service

Science (print ISSN 0036-8075; online ISSN 1095-9203) is published by the American Association for the Advancement of Science, 1200 New York Avenue NW, Washington, DC 20005. The title *Science* is a registered trademark of AAAS.

Copyright © 2015, American Association for the Advancement of Science

Downloaded from http://science.sciencemag.org/ on February 26, 2020